

1
2
3
4
5
6
7
8
9
10
11
12
13
14
15
16
17
18

Impact of proxies and prior estimates on data assimilation using isotope ratios for the climate reconstruction of the last millennium

Satoru Shoji¹, Atsushi Okazaki², and Kei Yoshimura³

¹The University of Tokyo, Kashiwa, Chiba, Japan.

²The Pennsylvania State University, University Park, Pennsylvania, United States.

³Institute of Industrial Science, The University of Tokyo, Kashiwa, Chiba, Japan.

Corresponding author: Satoru Shoji (shoji.satoru@s.nenv.k.u-tokyo.ac.jp)

Key Points:

- The climate reconstruction by data assimilation shows annual variations in surface air temperature and precipitation amount during 850–2000.
- Comparison of the spatiotemporal differences of the climate reconstruction due to prior estimates.
- Validation of the impacts of proxies in the results of reproduced past El Niño cases from 1971 to 2000.

19 **Abstract**

20 In climate reconstructions by data assimilation, the sensitivities to both proxies and prior estimates
21 need to be taken into account because models are uncertain and proxies are limited
22 spatiotemporally. This study examines these sensitivities using multiple climate model
23 simulations and different combinations of proxies (corals, ice cores, and tree-ring cellulose).
24 Experiments were conducted based on an offline data assimilation approach. These experiments
25 show annual variations in the global distribution of surface air temperature and precipitation range
26 from 850 to 2000. The results indicate that standard deviations of surface air temperature and
27 precipitation amount during the entire period differ by up to 50% due to prior estimates.
28 Experiments with different types of proxies show that the El Niño-like distribution of positive
29 anomalies in the central to eastern tropical Pacific can be reproduced adequately in experiments
30 with corals, but not in experiments without corals. The correlation coefficient of the NINO.3 index
31 from 1971 to 2000 between experiments with corals and the Japanese 55-year Reanalysis
32 (JRA-55) were 0.79 at maximum, while the correlation coefficient between experiments without
33 corals and JRA-55 were 0.20 at maximum.

34 **1 Introduction**

35 Climate reconstruction enables us to understand past climate changes. A variety of climate
36 proxies have been used for long-term climate reconstruction (Jones et al., 2001; Mann and Jones,
37 2003; Mann et al., 2008). As an example of proxies, tree rings provide information on the density
38 of rings and ring width, as well as carbon, oxygen, and hydrogen isotopes (McCarroll and Loader,
39 2004; Sheppard, 2010). Oxygen and hydrogen isotopes are called water isotopes. Due to the
40 physical and chemical processes associated with water, the water isotope ratio changes under the
41 influence of temperature, precipitation amount, moisture transport, etc. Based on the relationship
42 between temperature and water isotope ratio (Dansgaard, 1964), we can estimate temperature
43 using empirical equations. Water isotope ratios are recorded in not only tree rings but also various
44 types of proxies such as corals and ice cores (e.g., Felis and Pätzold, 2004; Kawamura, et al.,
45 2017).

46 Recently, data assimilation has been introduced into climate reconstruction. Data
47 assimilation provides optimal estimates based on both proxy data and climate model simulations.
48 So far, fluctuations in climate variables have been reproduced at time intervals from month to year
49 (Hakim et al., 2016; Franke et al., 2017; Steiger et al., 2018; Tardif et al., 2019).

50 However, in most research, before the data assimilation procedure, water isotope ratios
51 were converted into climate variables such as annually averaged temperature based on an
52 empirical equation. Variations in water isotope ratios are influenced by not only temperature but
53 also precipitation amount. If the reconstructed temperature is used for data assimilation,
54 information from other factors would be overlooked. Moreover, it is uncertain whether empirical
55 equations based on the current climate state are valid in the past climate state.

56 To solve these problems, Okazaki and Yoshimura (2017) used an isotopes-incorporated
57 climate model and assimilated oxygen isotope ratios directly. The data assimilation method
58 followed those of Bhend et al. (2012) and Steiger et al. (2014). The surface air temperature and
59 precipitation amount for the last 130 years were validated. The results showed the feasibility of
60 climate reconstruction based on data assimilation using oxygen isotope ratios of corals, ice cores,
61 and tree-ring cellulose. However, the difference due to prior estimates was not validated in

62 Okazaki and Yoshimura (2017). As these results can be changed by prior estimates, the impact of
63 using different climate models needs to be tested.

64 The current study uses multiple climate model simulations based on the method of Okazaki
65 and Yoshimura (2017). Annual variations in climate variables are reconstructed over the past 1000
66 years, and differences due to prior estimates are investigated. We also test the impacts of proxies
67 with experiments using different combinations of proxies. In this data assimilation method,
68 reconstructed fluctuations are dependent on the impacts of proxies because prior estimates are
69 constant throughout the entire target period. The impacts of proxies need to be evaluated, as well
70 as differences due to prior estimates, to improve climate reconstruction by data assimilation.

71 In Section 2, the models, proxy data, climate data sets, data assimilation, and experimental
72 design are introduced. In Section 3, we show the results of proxy data assimilation. We discuss
73 differences by climate models and the impacts of proxies in Section 4, and end by presenting our
74 conclusions in Section 5.

75 **2 Materials and Methods**

76 **2.1 Models**

77 To validate the influence of the difference due to prior estimates, we use two
78 isotopes-incorporated atmospheric general circulation models to make prior estimates. One is the
79 isotopes-incorporated model for interdisciplinary research on climate (MIROC5-iso; Okazaki
80 and Yoshimura, 2019) based on the atmospheric component of MIROC5 (Watanabe et al.,
81 2010). The other is the isotopes-incorporated global spectral model (IsoGSM; Yoshimura et al.,
82 2008) based on the Scripps Experimental Climate Prediction Center's (ECPC) GSM (Kanamitsu
83 et al., 2002). For climate model simulations, two datasets of sea surface temperature (SST) and
84 sea ice were used. They are provided by the historical run of the Coupled Model Intercomparison
85 Project Phase 5 (CMIP5; Taylor et al., 2007); one is from the atmosphere-ocean coupled version
86 of MIROC5, while the other is from the Community Climate System Model (CCSM4; Gent et
87 al., 2011). Each simulation period is of 130 years. The method for making prior estimates is
88 detailed in section 2.4.

89
90 In this study, proxy models for corals (Liu et al., 2014) and tree-ring cellulose (Roden et al.,
91 2000) were used. Isotope ratios of corals, ice cores, and tree-ring cellulose were calculated from
92 climatic variables of the climate model simulations. Each proxy model is described here.

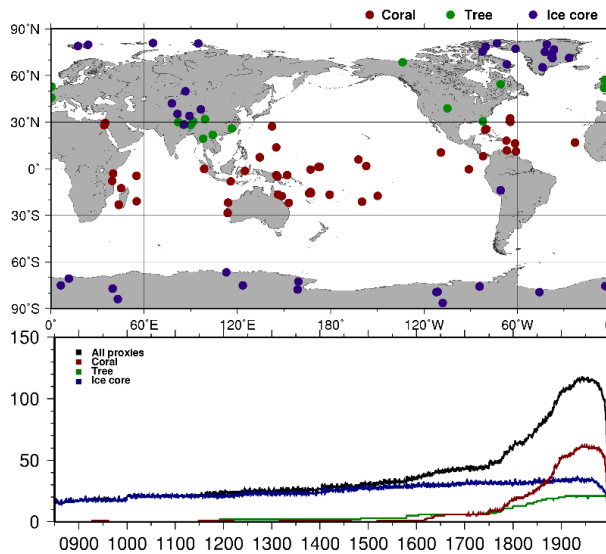
93 To calculate the isotope ratios of corals, we used monthly precipitation, evaporation, SST, and
94 oxygen isotope ratio data in the seawater studied LeGrande and Schmidt (2006). Coral isotope
95 ratios are based on the linear combination of SST and oxygen isotope ratio data in seawater. In
96 calculating the isotope ratio in seawater, the isotopic mass balance is considered using
97 precipitation and evaporation.

98
99 Isotope ratios of ice cores are assumed to be equal to those in precipitation. The isotope ratios
100 change after snow deposition (Hoshina et al., 2014) and the governing post-depositional
101 processes can vary by region. As it is difficult to reflect the entire process, isotope ratios in
102 precipitation calculated from the climate models were used without any post-depositional
103 processes when assimilating the isotope ratios of ice cores.

105 A model developed by Roden et al. (2000) was used to obtain isotope ratios of tree-ring
 106 cellulose. The monthly isotope ratios were calculated from climatic variables such as
 107 precipitation and evapotranspiration. To estimate the annual isotope ratios, the monthly isotope
 108 ratios were weighted by climatological net primary production (NPP) provided by the National
 109 Aeronautics and Space Administration National Aeronautics and Space Administration (NASA).
 110

111 2.2 Proxy data used in this study

112 We used 129 isotopic proxy data (65 corals, 43 ice cores, and 21 tree-ring cellulose) archived at
 113 the National Oceanic and Atmospheric Administration (NOAA;
 114 <https://www.ncdc.noaa.gov/data-access/paleoclimatology-data>) and the 2k Network of the
 115 International Geosphere-Biosphere Programme Past Global Changes (PAGES 2k; Ahmed et al.,
 116 2013). The spatial and temporal distribution of the proxies is shown in Figure 1. We assimilate
 117 the annual mean oxygen isotopic ratios of corals, ice cores, and tree-ring cellulose from 850 to
 118 2000. All proxy data were processed in the same way as Okazaki and Yoshimura (2017) before
 119 data assimilation, and their errors were set to 0.50. Note that isotope ratios of real proxies and
 120 modeled proxies were normalized over the same period in Okazaki and Yoshimura (2017),
 121 whereas they were normalized over different periods in this study.
 122



123
 124 **Figure 1.** Spatial and temporal distribution of proxies used in this study from 850 to 2000. Each
 125 color indicates corals (red), ice cores (blue), and tree-ring cellulose (green), respectively.
 126

127 2.3 Reference climate datasets used for comparison

128 Two types of climate datasets were utilized to validate this climate reconstruction. One is
 129 provided by the Climatic Research Unit (CRU; Harris et al., 2020). The data cover the entire
 130 land area except for Antarctica from 1901 with a spatial resolution of 0.5° . The surface air
 131 temperature [$^\circ\text{C}$] and precipitation [mm/day] of CRU were used for validation. The other data
 132 come from the Japanese 55-year Reanalysis (JRA-55; Kobayashi et al., 2015) by the Japan
 133 Meteorological Agency (JMA). They produce global climate variables at intervals of 1.25° . The
 134 analysis data from 1958 are available. We used temperature [K] from the surface analysis fields

135 and total precipitation [mm/day] from two-dimensional average diagnostic fields. Before
136 comparison with the results, each climate variable was averaged annually because annual
137 analyses were computed in this data assimilation.
138

139 2.4 Data assimilation method

140 Figure 2 shows the schematic of this proxy data assimilation. In this study, we follow the method
141 of Okazaki and Yoshimura (2017) using the so-called offline data assimilation approach (e.g.
142 Bhend et al., 2012; Steiger et al., 2014) based on the sequential ensemble square root filter
143 (EnSRF; Whitaker and Hamill, 2002), a variant of the ensemble Kalman filter (EnKF; Evensen,
144 2003). Note that the offline data assimilation does not ensure the temporal continuity of analyses
145 because prior estimates were constructed from existing climate model simulations.
146

147 We use a 130-year single run (1871-2000) to construct the prior estimates. The annual means are
148 calculated from the simulation, and each mean of 130 years is regarded as an ensemble member.

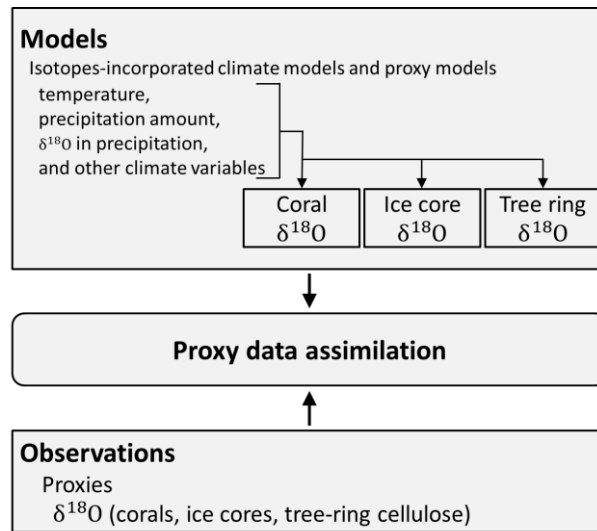
149 The same ensemble members were used for each year of the target period from 850 to 2000.

150 Therefore, prior estimates used for data assimilation are constant throughout the entire period.

151 The equations for data assimilation are as follows:

$$\mathbf{X}_a = \mathbf{X}_b + \mathbf{K}[\mathbf{y} - H(\mathbf{X}_b)]$$
$$\mathbf{K} = \mathbf{B}\mathbf{H}^T[\mathbf{H}\mathbf{B}\mathbf{H}^T + \mathbf{R}]^{-1}$$

152 \mathbf{X}_a is the state vector of the analysis and \mathbf{X}_b is that of the background estimate. Eight variables,
 153 namely, surface air temperature, precipitation amount, evapotranspiration, relative humidity,
 154 surface pressure, and three types of isotope ratios (corals, ice cores, and tree-ring cellulose) are
 155 included in the state vector. Vector \mathbf{y} consists of proxy data observations. Function H is the
 156 observation operator that converts the model state to the observation state. Innovation, $\mathbf{y} - H(\mathbf{X}_b)$,
 157 is the difference between the observations and the background estimates. The matrix \mathbf{K} , the
 158 Kalman gain, weights the innovation and transforms it into state space. Matrix \mathbf{B} is the background
 159 error covariance matrix, and \mathbf{R} is the observation error covariance matrix. Matrix \mathbf{H} is a linearized
 160 H around the background mean. In the offline data assimilation, both \mathbf{B} and \mathbf{R} are constant over
 161 time. Following Steiger et al. (2014), a localization function (Gaspari and Cohn, 1999) with a scale
 162 of 12,000 km is used and applied to the gain \mathbf{K} .



163 **Figure 2.** Schematic of this proxy data assimilation.
 164

165

166 2.5 Experimental design

167 We tested whether the results depended on the background fields with three simulations (Table
 168 1). The first one was based on MIROC5-iso forced by the SST of MIROC5. The second one was
 169 based on IsoGSM forced by the SST of MIROC5. The last was based on the IsoGSM forced by
 170 SST of CCSM4.

171

172 **Table 1.**
 173 *Experimental design.*

Experimental name	MIROC5-iso-m	IsoGSM-m	IsoGSM-c
Model	MIROC5-iso	IsoGSM	IsoGSM
SST for simulation	MIROC5	MIROC5	CCSM4
Reconstruction period	850-2000	850-2000	850-2000

174

175 First, we conducted experiments that reconstructed climate fields from 850 to 2000 using all 129
 176 proxies (ALL). Next, we limited the proxies used for data assimilation to investigate the impacts
 177 of proxies on analysis. The impacts of proxies were validated based on experiments using corals
 178 (C), ice cores (I), tree-ring cellulose (T), corals and ice cores (CI), corals and tree-ring cellulose
 179 (CT), and ice cores and tree-ring cellulose (IT). This study focused on experiments C and IT
 180 because the differences in the impacts of proxies are clear between these two types of
 181 experiments.

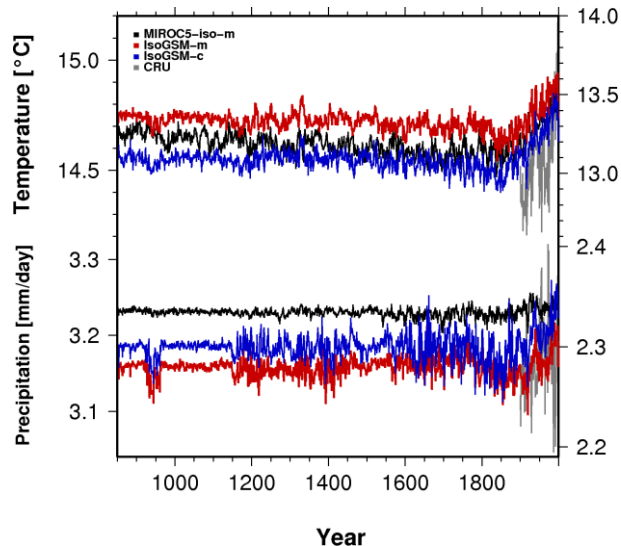
182

183 3 Results

184 3.1 Experiments using different prior estimates in the last millennium

185 In Section 3.1, the results of the experiment ALL are focused. Figure 3 shows the annual
 186 variations in the global mean surface air temperature [$^{\circ}\text{C}$] and precipitation amount [mm/day]
 187 from 850 to 2000. The fluctuations of the surface air temperature are similar to one another.
 188 Similarly, the precipitation amounts of IsoGSM-m and IsoGSM-c also varied. On the other hand,
 189 the precipitation amount of MIROC5-iso-m did not change as greatly as those of IsoGSM-m and
 190 IsoGSM-c. In the 10th century and latter half of the 12th to 16th centuries, fluctuations in
 191 precipitation amount are represented in the results of IsoGSM-m and IsoGSM-c; this fluctuation
 192 is not shown in MIROC5-iso-m.

193



194

195 **Figure 3.** Annual variations of reconstructed global mean surface air temperature [$^{\circ}\text{C}$] (upper)
 196 and precipitation amount [mm/day] (bottom) from 850 to 2000 (left axis). Each line shows the
 197 result of MIROC5-iso-m (black), IsoGSM-m (red), and IsoGSM-c (blue). Gray lines indicate
 198 CRU from 1901 to 2000 (right axis).

199

200 The averages and standard deviations of the global mean surface air temperature and
 201 precipitation amount are shown in Table 2. In the three experiments, the standard deviations in
 202 surface air temperature and precipitation amount in the 10th century were smaller than those in
 203 the 20th century, as shown in Figure 3. However, the differences in standard deviations of surface
 204 air temperature and precipitation amounts between the 10th and 20th centuries vary in each

205 experiment. Standard deviations of surface air temperature and precipitation amount in the 10th
 206 century are 33–57% and 33–50%, respectively, compared with those in the 20th century. During
 207 the entire target period, the standard deviations of surface air temperature did not differ
 208 significantly in each experiment. However, in the case of precipitation amount, the standard
 209 deviations of MIROC5-iso-m are less than half those of IsoGSM-m and IsoGSM-c.
 210 In the 20th century, the results were evaluated with the data of CRU. In the case of CRU, the
 211 standard deviations of the global mean surface air temperature and precipitation amount are 0.26
 212 °C and 0.04 mm/day, respectively. Compared with the standard deviations of CRU, those of the
 213 three experiments are 27–35% and 25–75% respectively for surface air temperature and
 214 precipitation amount. The fluctuation range of this study is smaller than that of CRU. However,
 215 the warming trend in the 20th century is clearly indicated in the three experiments, as well as in
 216 the case of CRU.

217

Table 2.

219 *Averages (left) and standard deviations (right) of global mean surface air temperature [°C] (top)*
 220 *and precipitation amount [mm/day] (bottom). Values in the 10th century, 20th century, and from*
 221 *850 to 2000 are shown.*

Surface air temperature	10C		20C		850–2000	
MIROC5-iso-m	14.62	0.04	14.71	0.07	14.62	0.06
IsoGSM-m	14.73	0.03	14.79	0.07	14.72	0.05
IsoGSM-c	14.54	0.03	14.66	0.09	14.55	0.06
CRU	-	-	13.09	0.26	-	-

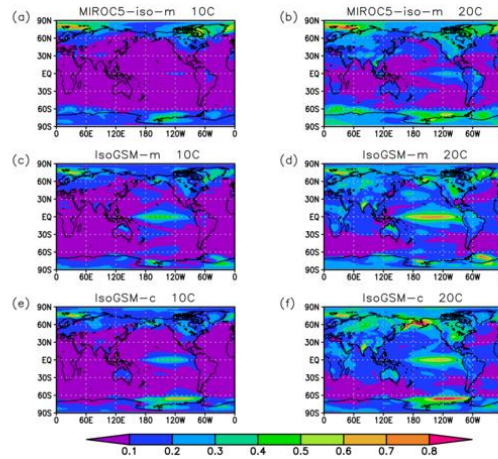
Precipitation amount	10C		20C		850–2000	
MIROC5-iso-m	3.23	0.003	3.24	0.01	3.23	0.01
IsoGSM-m	3.15	0.01	3.17	0.02	3.16	0.01
IsoGSM-c	3.18	0.01	3.20	0.03	3.18	0.02
CRU	-	-	2.29	0.04	-	-

222

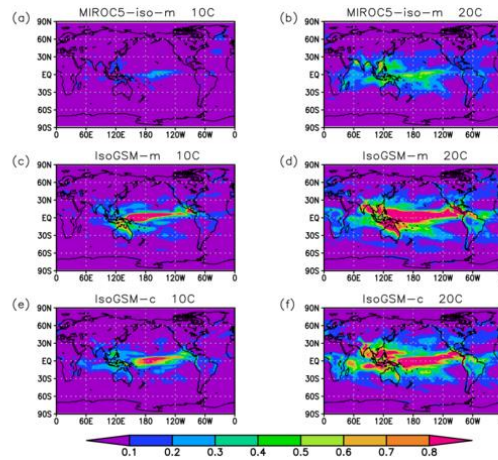
223

224 Figure 4 and Figure 5 show the spatial distribution of standard deviations of surface air
 225 temperature and precipitation amount. In Figure 4, the three experiments show high variability in
 226 the Arctic and Antarctic regions and Northern America in the 10th century. In the case of
 227 IsoGSM-m and IsoGSM-c, high variations were also observed in the tropical Pacific. In the 20th
 228 century, variability in the tropical Pacific and the Arctic and Antarctic regions was higher than in
 229 the 10th century. In addition, the high value areas spread from the Arctic regions to most of the
 230 Northern Hemisphere in the three experiments. In Figure 5, values are high in the tropical Pacific
 231 and higher in IsoGSM-m and IsoGSM-c than in MIROC5-iso-m. In the three experiments,
 232 values were higher in the 20th century than in the 10th century.

233



234 **Figure 4.** Spatial distribution of standard deviations of surface air temperature [$^{\circ}\text{C}$] in the 10th
 235 (left) and 20th (right) century. The results of MIROC5-iso-m (top), IsoGSM-m (middle), and
 236 IsoGSM-c (bottom) are shown.
 237
 238



239 **Figure 5.** Same as in Figure 4 but for precipitation amount [mm/day].
 240
 241

242 3.2 Validation of reconstructed climate fields

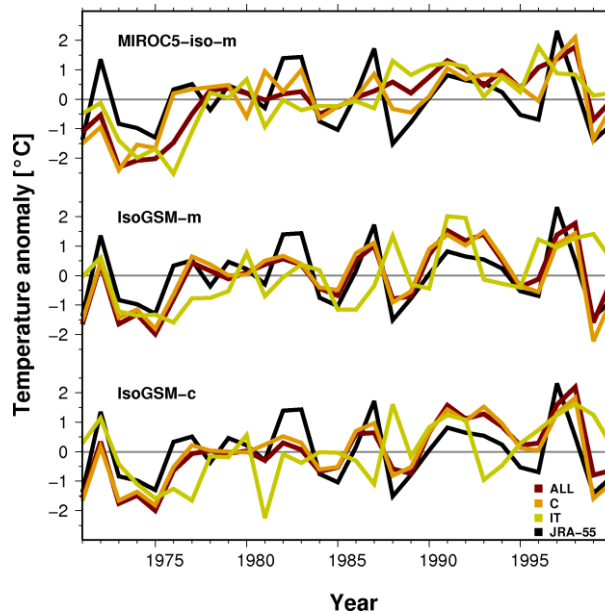
243 To validate the climate field reconstructed in this study, we focus on El Niño from 1971 to 2000
 244 (Table 3). Figure 6 shows annual variations of standardized surface air temperature anomalies in
 245 NINO.3. The values of each result are positive in some El Niño years as seen in JRA-55. The
 246 fluctuations of IsoGSM-m are closer to that of JRA-55 especially. Compared with each
 247 experiment, the fluctuations of experiment ALL and C are more similar to that of JRA-55.
 248

249 **Table 3.**
 250 *El Niño from 1971 to 2000 announced by JMA.*

	Period (year.month)	Max [$^{\circ}\text{C}$]
E1	1972.4–1973.3	+2.7
E2	1976.5–1977.3	+1.5
E3	1982.3–1983.8	+3.3

E4	1986.8–1988.1	+1.7
E5	1991.3–1992.7	+1.6
E6	1997.3–1998.5	+3.6

251



252

253 **Figure 6.** Standardized annual variations of surface air temperature anomalies [°C] in NINO.3
 254 from 1971 to 2000. The results of MIROC5-iso-m (top), IsoGSM-m (middle), and IsoGSM-c
 255 (bottom) are shown. Each color represents experiment ALL (red), C (orange), and IT (yellow),
 256 respectively. Black lines indicate JRA-55.

257

258 Table 4 shows the root mean square differences (RMSD) between each result and JRA-55,
 259 correlation coefficients (r) with JRA-55, and standard deviations (σ). These values are based on
 260 the annual variations of the surface air temperature anomalies from 1971 to 2000. As seen in
 261 Table 4, the RMSD of experiment C is the smallest, while that of experiment IT is the largest for
 262 each result. Comparing the results of experiments ALL and IT, each RMSD differed by 10–27%.
 263 The RMSD of IsoGSM-m is smaller than those of MIROC5-iso-m and IsoGSM-c. The
 264 correlation coefficients of IsoGSM-m and IsoGSM-c are higher than those of MIROC5-iso-m.
 265 Each correlation coefficient of experiment C is higher than those of experiments ALL and IT.
 266 The ratios of standard deviations (this study/JRA-55) are about 22–35% in MIROC5-iso-m. In
 267 the cases of IsoGSM-m and IsoGSM-c, these ratios are about 30–94%. The standard deviations
 268 of experiments ALL and C are higher than those of experiment IT. Table 5 shows years when the
 269 annual surface air temperature anomalies in NINO.3 exceed $+\sigma$ from 1971 to 2000. The values
 270 are evaluated after standardization. The values of JRA-55 are higher $+\sigma$ in the El Niño years of
 271 E1, E3, E4, and E6. On the other hand, El Niño E1, E4, E5, and E6 are indicated in this study.
 272 The years in which El Niño events did not occur are also pointed out. El Niño E6 is strongest in
 273 this period (Table 3). It is regarded as the largest El Niño in the 20th century. This case is
 274 reproduced in experiments ALL and C but not in experiment IT.

275

276 **Table 4.**

277 *Values of root mean square difference (RMSD) [°C] between each result and JRA-55, correlation*
 278 *coefficients (r) with JRA-55, and standard deviations (σ) [°C] based on the annual variations of*

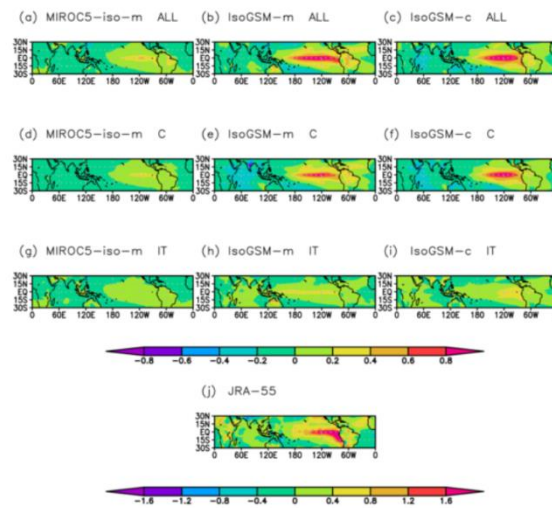
279 *surface air temperature anomalies in NINO.3 from 1971 to 2000. Each result is based on*
 280 *MIROC5-iso-m (left), IsoGSM-m (middle), and IsoGSM-c (right).*

	RMSD [°C]		r			σ [°C]			
ALL	0.57	0.40	0.45	0.46	0.78	0.71	0.22	0.59	0.53
C	0.55	0.40	0.41	0.65	0.79	0.77	0.15	0.59	0.56
IT	0.63	0.63	0.65	0.14	0.20	0.05	0.14	0.23	0.19
JRA-55	-		-			0.63			

281
 282 **Table 5.**
 283 *Years in which surface air temperature anomalies in NINO.3 exceed +σ. The underlined years*
 284 *imply El Nino years.*

	MIROC5-iso-m	IsoGSM-m	IsoGSM-c
ALL	<u>1991, 1992, 1996,</u> <u>1997, 1998</u>	<u>1987, 1991, 1992,</u> <u>1993, 1997, 1998</u>	<u>1991, 1992, 1993,</u> <u>1997, 1998</u>
C	<u>1981, 1997, 1998</u>	<u>1987, 1991, 1992,</u> <u>1993, 1997, 1998</u>	<u>1991, 1992, 1993,</u> <u>1997, 1998</u>
IT	<u>1988, 1990, 1991,</u> <u>1992, 1996</u>	<u>1988, 1991, 1992,</u> <u>1996, 1998, 1999</u>	<u>1972, 1988, 1991,</u> <u>1992, 1997, 1998,</u> 1999
JRA-55	<u>1972, 1982, 1983, 1987, 1997</u>		

285
 286 Figure 7 shows the spatial distribution of surface air temperature anomalies in the tropical Pacific
 287 in 1997. Anomalies are defined based on 30 years from 1971 to 2000. The figure of JRA-55
 288 represents a positive anomaly in the central to eastern tropical Pacific and a negative anomaly in
 289 the western tropical Pacific. We can find a similar spatial distribution in each result of
 290 experiments ALL and C, although the positive anomaly is smaller compared with JRA-55. On
 291 the other hand, the results of experiment IT do not show a positive anomaly in the tropical
 292 Pacific and a negative anomaly in the western tropical Pacific.



293
 294 **Figure 7.** Spatial distribution of surface air temperature anomaly [°C] in the tropical Pacific in
 295 1997. The results of this study are represented in Figure (a–i), and JRA-55 is in (j). Figures (a–c)
 296 represent experiment ALL, (d–f) experiment C, and (g–i) experiment IT. The results of

297 MIROC5-iso-m (left), IsoGSM-m (middle), and IsoGSM-c (right) are shown. Note that the color
298 bar of JRA-55 is different from the other.
299

300 **4 Discussion**

301 4.1 Difference due to prior estimates

302 The difference due to prior estimates is indicated in Figure 3. In the 10th century and the latter
303 half of the 12th to 16th centuries, fluctuations in the global mean precipitation of IsoGSM-m and
304 IsoGSM-c were larger than that of MIROC5-iso-m. In the same period, the number of coral
305 proxies increased (Figure 1). As prior estimates are constant for the entire target period in this
306 method, the fluctuations are dependent on the impacts of proxies. The results indicated that coral
307 proxies can significantly influence the precipitation fluctuations of IsoGSM-m and IsoGSM-c.
308 The difference due to these prior estimates is also shown in Figure 4 and Figure 5. In the tropical
309 Pacific, the spatial distribution of MIROC5-iso-m is different from that of IsoGSM-m and
310 IsoGSM-c. Compared with MIROC5-iso-m, the results of IsoGSM-m and IsoGSM-c represent
311 higher values in the tropical Pacific where coral proxies are available. This suggests the strong
312 impact of coral proxies on the spatial distribution of IsoGSM-m and IsoGSM-c.

313
314 The impact of coral proxies on the results of IsoGSM-m and IsoGSM-c is also shown in Figure
315 6. Although El Niño events did not occur, the positive anomaly was higher than $+\sigma$ in 1993.
316 Confirming the spatial distribution of JRA-55, a positive anomaly was observed within 180° to
317 150°W in the tropical Pacific in 1993. This influence may be reflected in the results of
318 IsoGSM-m and IsoGSM-c, which are sensitive to coral proxies.

319 4.2 Impacts of proxies

320 We compare the results of experiments ALL, C, and IT, and verify the impacts of proxies. The
321 fluctuations in the NINO.3 index, such as JRA-55, can be reproduced by experiments ALL and C
322 (Figure 6). In particular, the values in 1997 and 1998 exceeded $+\sigma$ in eight out of nine
323 experiments. El Niño E6 was one of the largest cases in the 20th century and can be represented
324 better than other cases because its influence spread widely and reflected strongly on coral proxies
325 in the tropical Pacific. Coral proxies play an important role in reproducing past El Niño. Cobb et
326 al. (2003) revealed fluctuations in oxygen isotope ratios over the last 1100 years based on coral
327 proxies in the central tropical Pacific. They analyzed the strength and frequency of El Niño in the
328 past and indicated that coral proxies in the tropical Pacific record the information of the past El
329 Niño. Information on coral proxies can be reflected in the results of the current study. In Table 4,
330 each RMSD is high in experiment IT, and low in experiments ALL, and C. The decrease in
331 RMSD is largely dependent on coral proxies. In addition, correlation coefficients were high in
332 experiments ALL and C and low in experiment IT. Thus, coral proxies are effective for the
333 reconstruction of past El Niño events using this method.

334
335 The importance of coral proxies for past El Niño reconstruction is also indicated in Figure 7. The
336 results of experiments ALL and C can reproduce positive anomalies in the central and eastern
337 tropical Pacific. However, in experiment IT, the positive anomaly is small and the spatial
338 distribution of El Niño cannot be shown.

339

340 **5 Conclusions**

341 This study showed annual variations in the global distribution of surface air temperature and
342 precipitation amount from 850 to 2000 by proxy data assimilation. We used
343 isotopes-incorporated climate models and proxy models to assimilate oxygen isotope ratios of
344 corals, ice cores, and tree-ring cellulose. Experiments based on different prior estimates and
345 proxies were conducted to evaluate sensitivity.

346
347 The differences due to prior estimates were shown spatiotemporally. Although the fluctuations of
348 global mean surface air temperature were similar in the three experiments, those of the
349 precipitation amount were different between MIROC5-iso-m and IsoGSM-m (IsoGSM-c). The
350 standard deviations of the precipitation amount of IsoGSM-m and IsoGSM-c were twice as large
351 as that of MIROC5-iso-m during 850–2000. The fluctuations in the precipitation amounts of
352 IsoGSM-m and IsoGSM-c corresponded to the change in the number of coral proxies. In
353 addition, surface air temperature and precipitation amount in the tropical Pacific were high in
354 IsoGSM-m and IsoGSM-c, and low in MIROC5-iso-m. These results suggest that coral proxies
355 significantly influenced the results of IsoGSM-m and IsoGSM-c.

356
357 The impacts of proxies were shown in the results of reproduced past El Niño cases. In
358 experiments ALL and C, the El Niño-like positive anomaly of surface air temperature in the
359 tropical Pacific was reproduced well and fluctuations of surface air temperature anomalies in
360 NINO.3 were close to the case of JRA-55. The results indicated that coral proxies were effective
361 in reconstructing the past El Niño patterns.

362

363 **Acknowledgments**

364 This study was supported by the Japan Society for the Promotion of Science (JSPS) via
365 Grants-in-Aid 18H03794 and 16H06291, JRPs-LEAD with DFG, and the Integrated Research
366 Program for Advancing Climate Models (TOUGOU) Grant Number JPMXD0717935457, ArCS,
367 and DIAS from the Ministry of Education, Culture, Sports, Science and Technology (MEXT),
368 Japan.

369

370 **Open Research**

371 The results of this study are available from <https://doi.org/10.5281/zenodo.4320464>.

372

373 **References**

- 374 Ahmed, M., Anchukaitis, K. J., Asrat, A., Borgaonkar, H. P., Braida, M., Buckley, B. M., et al.
375 (2013). Continental-scale temperature variability during the past two millennia. *Nature*
376 *geoscience*, 6(5), 339–346.
- 377 Bhend, J., Franke, J., Folini, D., Wild, M., & Brönnimann, S. (2012). An ensemble-based
378 approach to climate reconstructions. *Climate of the Past*, 8.3: 963–976.

- 379 Cobb, K. M., Charles, C. D., Cheng, H., & Edwards, R. L. (2003). El Niño/Southern Oscillation
380 and tropical Pacific climate during the last millennium. *Nature*, 424(6946), 271.
- 381 Dansgaard, W. (1964). Stable isotopes in precipitation. *Tellus*, 16.4: 436–468.
- 382 Evensen, G. (2003). The ensemble Kalman filter: Theoretical formulation and practical
383 implementation. *Ocean dynamics*, 53(4), 343–367.
- 384 Felis, T., & Pätzold, J. (2004). Climate reconstructions from annually banded corals. *Global
385 environmental change in the ocean and on land*, 205–227.
- 386 Franke, J., Brönnimann, S., Bhend, J., & Brugnara, Y. (2017). A monthly global paleo-reanalysis
387 of the atmosphere from 1600 to 2005 for studying past climatic variations. *Scientific data*,
388 4, 170076.
- 389 Gaspari, G., & Cohn, S. E. (1999). Construction of correlation functions in two and three
390 dimensions. *Quarterly Journal of the Royal Meteorological Society*, 125(554), 723–757.
- 391 Gent, P. R., Danabasoglu, G., Donner, L. J., Holland, M. M., Hunke, E. C., Jayne, S. R., et al.
392 (2011). The community climate system model version 4. *Journal of Climate*, 24(19),
393 4973–4991.
- 394 Hakim, G. J., Emile - Geay, J., Steig, E. J., Noone, D., Anderson, D. M., Tardif, R., et al. (2016).
395 The last millennium climate reanalysis project: Framework and first results. *Journal of
396 Geophysical Research: Atmospheres*, 121(12), 6745–6764.
- 397 Harris, I., Osborn, T. J., Jones, P., & Lister, D. (2020). Version 4 of the CRU TS monthly
398 high-resolution gridded multivariate climate dataset. *Scientific data*, 7(1), 1–18.
- 399 Hoshina, Y., Fujita, K., Nakazawa, F., Iizuka, Y., Miyake, T., Hirabayashi, M., et al. (2014).
400 Effect of accumulation rate on water stable isotopes of near-surface snow in inland
401 Antarctica. *Journal of Geophysical Research: Atmospheres*, 119(1), 274–283.
- 402 Jones, P. D., Osborn, T. J., & BRIFFA, K. R. (2001). The evolution of climate over the last
403 millennium. *Science*, 292(5517), 662–667.
- 404 Kanamitsu, M., Kumar, A., Juang, H. M. H., Schemm, J. K., Wang, W., Yang, F., et al. (2002).
405 NCEP dynamical seasonal forecast system 2000. *Bulletin of the American Meteorological
406 Society*, 83(7), 1019–1038.
- 407 Kawamura, K., Abe-Ouchi, A., Motoyama, H., Ageta, Y., Aoki, S., Azuma, N., et al. (2017).
408 State dependence of climatic instability over the past 720,000 years from Antarctic ice
409 cores and climate modeling. *Science advances*, 3(2), e1600446.
- 410 Kobayashi, S., Ota, Y., Harada, Y., Ebata, A., Moriya, M., Onoda, H., et al. (2015). The JRA-55
411 reanalysis: General specifications and basic characteristics. *Journal of the Meteorological
412 Society of Japan*. Ser. II, 93(1), 5–48.
- 413 LeGrande, A. N., & Schmidt, G. A. (2006). Global gridded data set of the oxygen isotopic
414 composition in seawater. *Geophysical Research Letters*, 33, L12604,
415 doi:10.1029/2006GL026011.
- 416 Liu, G., Kojima, K., Yoshimura, K., & Oka, A. (2014). Proxy interpretation of coral-recorded
417 seawater $\delta^{18}\text{O}$ using 1-D model forced by isotopes-incorporated GCM in tropical oceanic
418 regions. *Journal of Geophysical Research: Atmospheres*, 119(21), 12,021–12,033.
- 419 Mann, M. E., & Jones, P. D. (2003). Global surface temperatures over the past two millennia.
420 *Geophysical Research Letters*, 30(15) 1820, doi:10.1029/2003GL017814.
- 421 Mann, M. E., Zhang, Z., Hughes, M. K., Bradley, R. S., Miller, S. K., Rutherford, S., & Ni, F.
422 (2008). Proxy-based reconstructions of hemispheric and global surface temperature
423 variations over the past two millennia. *Proceedings of the National Academy of Sciences*,
424 105(36), 13252–13257.

- 425 McCarroll, D., & Loader, N. J. (2004). Stable isotopes in tree rings. *Quaternary Science*
426 *Reviews*, 23(7-8), 771–801.
- 427 Okazaki, A., & Yoshimura, K. (2017). Development and evaluation of a system of proxy data
428 assimilation for paleoclimate reconstruction. *Climate of the Past*, 13(4), 379–393.
- 429 Okazaki, A., & Yoshimura, K. (2019). Global evaluation of proxy models for stable water
430 isotopes with realistic atmospheric forcing. *Journal of Geophysical Research:*
431 *Atmospheres*, 124(16), 8972–8993.
- 432 Roden, J. S., Lin, G., & Ehleringer, J. R. (2000). A mechanistic model for interpretation of
433 hydrogen and oxygen isotope ratios in tree-ring cellulose. *Geochimica et Cosmochimica*
434 *Acta*, 64(1), 21–35.
- 435 Sheppard, P. R. (2010). Dendroclimatology: extracting climate from trees. *Wiley*
436 *Interdisciplinary Reviews: Climate Change*, 1(3), 343–352.
- 437 Steiger, N. J., Hakim, G. J., Steig, E. J., Battisti, D. S., & Roe, G. H. (2014). Assimilation of
438 time-averaged pseudoproxies for climate reconstruction. *Journal of Climate*, 27.1: 426–
439 441.
- 440 Steiger, N. J., Smerdon, J. E., Cook, E. R., & Cook, B. I. (2018). A reconstruction of global
441 hydroclimate and dynamical variables over the Common Era. *Scientific data*, 5, 180086.
- 442 Tardif, R., Hakim, G. J., Perkins, W. A., Horlick, K. A., Erb, M. P., Emile-Geay, J., et al. (2019).
443 Last Millennium Reanalysis with an expanded proxy database and seasonal proxy
444 modeling. *Climate of the Past*, 15(4), 1251–1273.
- 445 Taylor, K. E., Stouffer, R. J., & Meehl, G. A. (2012). An overview of CMIP5 and the experiment
446 design. *Bulletin of the American Meteorological Society*, 93(4), 485–498.
- 447 Watanabe, M., Suzuki, T., O’ishi, R., Komuro, Y., Watanabe, S., Emori, S., et al. (2010).
448 Improved climate simulation by MIROC5: Mean states, variability, and climate sensitivity.
449 *Journal of Climate*, 23(23), 6312–6335.
- 450 Whitaker, Jeffrey S., & Hamill, T. M. (2002). Ensemble data assimilation without perturbed
451 observations. *Monthly Weather Review*, 130(7), 1913–1924.
- 452 Yoshimura, K., Kanamitsu, M., Noone, D., & Oki, T. (2008). Historical isotope simulation using
453 reanalysis atmospheric data. *Journal of Geophysical Research: Atmospheres*, 113,
454 D19108, doi:10.1029/2008JD010074.
- 455
456